ChemComm

COMMUNICATION

Check for updates

Multifunctional luminogens with synergy of aggregation-induced delayed fluorescence, two-photon absorption and photocurrent generation†

Abhijit Chatterjee,‡[a] Sundaravalli Narayanan,‡[a] Sachin Thorat,[ab] Ajay J. Malik,[c] Madan D. Ambhore, [ID][d] Aswini Narayanan,[ef] Anil Kumar Sihag,[a] Sukumaran Santhosh Babu, [ID][ef] Mayurika Lahiri [ID][c] and Partha Hazra [ID] ★[a]

In this study, we investigated the aggregation-induced delayed fluorescence (AIDF) properties of three luminogens – TN, TA, and TP. Our comprehensive theoretical analysis reveals a significant reduction in the ΔE_{ST} in their aggregated or solid-state, activating TADF, on a $\sim\mu s$ time-scale. Additionally, these luminogens demonstrate two-photon excited anti-Stokes photoluminescence emission and improved photocurrent generation, attributed to their strong charge transfer characteristics and longer singlet exciton lifetimes.

Thermally activated delayed fluorescence (TADF) emitters have attracted significant interest in recent years, particularly for their applications in organic optoelectronics for OLEDs.[1] While traditional TADF emitters effectively utilize electrogenerated excitons, their performance in non-doped OLEDs is often limited by a reduced photoluminescence quantum yield (PLQY) in solid or aggregated states.[2] To overcome this challenge, the aggregation-induced emission (AIE) strategy has been introduced,[3] giving rise to a new category of TADF emitters known as aggregation-induced delayed fluorescent (AIDF) emitters.[4] These AIDF emitters demonstrate high exciton utilization and impressive photoluminescence

efficiency in neat films, making them ideal for the development of highly efficient and stable non-doped OLEDs. Recent advancements, such as the molecular core–shell approach developed by Tang and co-workers, have achieved remarkable efficiency in AIDF-OLEDs, with a current efficiency of 61.4 cd A^{-1} and power efficiency of 42.8 lm W^{-1}.[5] Additionally, Chi and co-workers reported two TADF emitters featuring aggregation-induced emission based on a shamrock-shaped donor–acceptor structure, achieving a notable external quantum efficiency (EQE) of 38.7% in the sky-blue region.[6] Yasuda and co-workers further contributed with a series of *o*-carborane-based emitters, showcasing high PL quantum efficiencies of up to 97% in solid-state films, along with successful non-doped OLED device fabrication.[7] While AIDF emitters have primarily been applied to non-doped OLEDs, their significant charge transfer properties and longer emission lifetimes suggest potential benefits for other areas of organic electronics, such as anti-Stokes photoluminescence (ASPL) *via* two-photon absorption and efficient photocurrent generation. In this report, we present three novel AIDF luminogens **TN**, **TA**, and **TP** based on triphenylamine as the donor (Fig. 1a). These TPA-based compounds exhibit advantageous photoconductive and light-emitting properties, with enhanced conjugation improving exciton up-conversion and utilization.[8] Notably, all three emitters demonstrate two-photon activity in their aggregated and crystalline states, attributed to their large hyperpolarizability. Furthermore, they generate efficient photocurrent in the microampere (μA) range, marking them as the first AIDF emitters with this capability.

After a multi-step synthesis process (Scheme S1, ESI†), the luminogens have been purified by HPLC and characterized by ^{1}H NMR, ^{13}C NMR and HRMS analysis (see ESI†). In all three emitters, the triphenylamine (TPA) group acts as a donor, as evidenced by the frontier molecular orbital analysis, with the HOMO located on the TPA moieties (Fig. S1, ESI†). On the other hand, the LUMO is localised predominantly in the peripheral nitro-benzene moiety, ester carbonyl group, and phthalimide moiety in the case of **TN**, **TA**, and **TP**, respectively (Fig. S1, ESI†). The luminogens in toluene (30 μM) exhibit a strong absorption

[a] *Department of Chemistry, Indian Institute of Science Education and Research (IISER), Pune (411008), Maharashtra, India. E-mail: p.hazra@iiserpune.ac.in*

[b] *Innovation Campus Mumbai, BASF Chemicals India Pvt. Ltd., Plot No. 12, TTC Area, Thane Belapur Road, Turbhe, Navi Mumbai, 400705, Maharashtra, India*

[c] *Department of Biology, Indian Institute of Science Education and Research (IISER), Pune (411008), Maharashtra, India*

[d] *Department of Chemistry, Yeshwant Mahavidyalaya Nanded, Nanded, PIN-431602, Maharashtra, India*

[e] *Organic Chemistry Division, National Chemical Laboratory (CSIR-NCL), Dr Homi Bhabha Road, Pune-411 008, India*

[f] *Academy of Scientific and Innovative Research (AcSIR), Ghaziabad-201 002, India*

† Electronic supplementary information (ESI) available: Instrumentation, materials, experimental details, crystallographic data, characterization data, respective spectra, computational details (DFT), and optical properties in solid and solution states. Temperature-dependent studies, applications and author contributions are provided. CCDC 2387501, 2378737 and 2387502. For ESI and crystallographic data in CIF or other electronic format see DOI: https://doi.org/10.1039/d4cc05113k
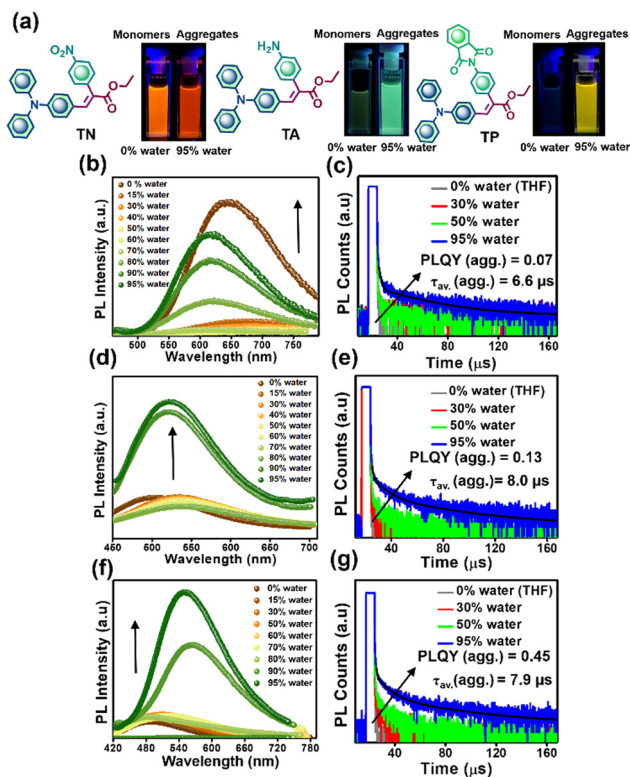
‡ Contributed equally as first authors.

Fig. 1 Molecular structures of (a) **TN**, (b) **TA**, and (c) **TP** along with monomer and aggregate emission (in cuvette). Emission spectra in binary THF/water mixtures for (b) **TN**, (d) **TA**, and (f) **TP**. Variation of lifetime (ex. 355 nm) in the ~µs time-scale with water content for (c) **TN**, (e) **TA** and (g) **TP**. Aggregate PLQY and average lifetime (at 95% water content) are mentioned inside the figure.

band in the 360–415 nm region (Fig. S2, ESI†), which is attributed to the $S_0–S_2$ transition for **TN** & **TP** and a combination of both $S_0–S_2$ and $S_0–S_1$ transitions for **TA**, based on the simulated absorption spectra obtained from TD-DFT calculation (Tables S4–S6 in ESI†). Noticeably, the emission features were found to be different for all three. **TN** in toluene emits in the yellow region ($\lambda_{max} \sim 550$ nm), whereas **TA** ($\lambda_{max} \sim 460$ nm) & **TP** ($\lambda_{max} \sim 465$ nm) emit in the cyan-blue region (Fig. S2, ESI†), probably attributed to an increased charge transfer character in **TN** due to its maximum conjugation length and S_1 state dipole moment (Fig. S3, ESI†). It is worth noting that the time-resolved photoluminescence (PL) decay of all the luminogens in solvents like-toluene and THF only shows a short ~ns component and is devoid of any longer component in the µs-ms time scale suggesting the absence of any triplet harvesting process in solution (Fig. S5 and S6, ESI†). However, an intriguing photophysical characteristic emerges in the aggregated state. All three molecules exhibit a profound aggregation induced enhanced emission (AIEE) behavior after an initial solvatochromic emission quenching up to ~60–70% of water content in THF. Impressively, at a water concentration of 95%, the emission profiles demonstrate enhancement of intensity of approximately 16-fold for **TN**, 5-fold for **TA**, and 10-fold for **TP**, as illustrated in Fig. 1b, d and f, Fig. S7 and Table S7 (Note S1) (ESI†). Importantly, the molecular aggregates formed at 95% water content exhibit PL

decay times in the microsecond (µs) range, with average lifetimes of 6.6 µs, 8.0 µs, and 7.9 µs for **TN**, **TA**, and **TP**, respectively (Fig. 1c, e and g). Here it is important to note that this long emission lifetime component was not prominent at very low water content ($<50\%$), when the aggregates are not formed. To investigate whether this aggregation behavior persists with a further increase in the extent of aggregation, we conducted additional studies on neat films and molecular crystals. The neat films of all three luminogens exhibit different emission features with **TN** emitting orange-red emission (maxima at ~ 620 nm), **TA** exhibiting cyan-green emission (maxima at ~ 520 nm) and **TP** exhibiting greenish yellow emission (maxima at ~ 545 nm) (Fig. S10 and Note S2 and S3, ESI†). In addition to the short $\sim$ ps–ns component (due to prompt $S_1–S_0$ emission), all three neat films exhibit a much longer emission lifetime of 27.3 µs, 8.64 µs, and 7.83 µs for **TN**, **TA**, and **TP**, respectively (Fig. S10, ESI†), suggesting the persistent role of aggregation in the emission process. Moreover, the molecular crystals of the respective emitters also emit in three different regions, with emission maxima at 620 nm, 525 nm, and 510 nm for **TN**, **TA**, and **TP**, respectively (Fig. S14, ESI†). Here also, along with a short $\sim$ ns component, a much longer emission lifetime is observed for all three crystals with an average lifetime of 104 µs, 86 µs, and 20 µs for **TN**, **TA**, and **TP**, respectively (Fig. S15, ESI†). Noticeably, the longer lifetime component exhibits a marked increase with the extent of aggregation, progressing from a THF-water binary mixture with 95% water content, to neat films, and ultimately to molecular crystals. This suggests a unique role of aggregation in the kinetics of this emission process. To determine the origin of such a longer lifetime, time-gated emission measurements were carried out. A significantly superimposed gated emission spectrum with the steady state emission profile indicates a probable occurrence of thermally activated delayed fluorescence (TADF) as in both cases the emission takes place from the lowest singlet S_1 state (Fig. S16, ESI†). This was further confirmed by photophysical investigation at cryogenic temperature. At 77 K, the TADF emission bands were found to be weakened with a red shift of the emission maxima suggesting the presence of phosphorescence emission from the lowest triplet T_1 state (Fig. S16, ESI†). From the peak position of the respective spectra, the $S_1–T_1$ energy gaps (ΔE_{ST}) were estimated to be 0.16 eV, 0.13 eV, and 0.10 eV for **TN**, **TA**, and **TP** crystals, respectively (Fig. S16, ESI†). Such low ΔE_{ST} values are particularly advantageous for facilitating TADF, as they imply a reduced activation barrier for the reverse intersystem crossing (RISC) process.[9] Noticeably, the experimentally obtained ΔE_{ST} values are in line with the delayed fluorescence lifetimes, with **TP** with the least ΔE_{ST} value exhibiting the minimum TADF lifetime. Furthermore, DF lifetimes were measured at a temperature of 77 K. In all three cases, the DF lifetime was found to be reduced at 77 K compared to room temperature due to an inefficient thermal up-conversion process at lower temperatures (Fig. S17, ESI†). Our designed luminogens, therefore are categorized as AIDF type molecules, as the spin–flip process only gets activated in the aggregated or solid state, not in the monomeric state. To understand the specific role of aggregation in the delayed fluorescence process, we performed a combined solvent-phase and QM/MM (quantum mechanics/molecular

mechanics) based DFT calculation (Fig. S18 and S19, ESI†). The solvent-based (IEFPCM/THF) calculation was used to model the monomeric/solution state, while the QM/MM calculation was used to model the aggregated/solid state. In the THF-based calculation, the theoretically calculated ΔE_{ST} values are found to be 0.27 eV, 0.95 eV, and 0.47 eV for **TN, TA**, and **TP**, respectively (Fig. S20, ESI†). These high ΔE_{ST} values are not suitable for efficient reverse intersystem crossing (RISC), which may be the reason for the emitters not showing TADF emission in the solution phase. Interestingly, calculations on the aggregated state convey a different story with much lowered ΔE_{ST} values of 0.03 eV, 0.06 eV, and 0.06 eV for **TN, TA**, and **TP**, respectively (Fig. 2). This narrow energy gap between the S_1 and T_1 states can make the reverse intersystem crossing (RISC) process much more efficient and presumably could be the reason for the activation of TADF in aggregated or solid states.

The aggregation-induced delayed fluorescence (AIDF) properties and long-range charge transfer characteristics of these luminogens were effectively utilized for photocurrent generation. In conventional organic fluorophores, singlet excitons typically decay on a picosecond to nanosecond timescale, resulting in limited exciton diffusion

lengths (L_S) constrained to just a few nanometers. Importantly, the exciton diffusion length is proportional to the square root of the singlet exciton lifetime (τ_S),[10] which restricts the efficiency of these materials as photocurrent generators. In contrast, our AIDF emitters exhibit significantly longer singlet lifetimes (in the microsecond regime), allowing for greater exciton diffusion lengths and facilitating efficient photocurrent generation. Consequently, all three luminogens produced photocurrents in the microampere range when excited with a 365–370 nm UV source (Fig. 3a). Notably, the drop-casted **TN** film exhibited the highest photocurrent of ∼4 μA, while **TP** demonstrated the lowest (Fig. 3a). Careful analysis of the photophysical properties reveals that the delayed fluorescence lifetimes in neat films follow the trend: **TN** (27.3 μs) > **TA** (8.64 μs) > **TP** (7.83 μs) (Fig. 3b). This indicates that **TN**, with its longest singlet exciton lifetime, achieves the greatest diffusion length, thereby maximizing its photocurrent generation capability.

Given their superior optical penetration, excellent spatial resolution, and minimal optical scattering, two-photon-excited organic luminogens have garnered significant interest compared to typical one-photon-excited fluorophores.[11] These two-photon active materials are especially valuable for cell imaging because they cause the least amount of damage to the target cell.[12] Given the extensive π-conjugated structures and strong charge transfer properties of our luminogens, which contribute to significant hyperpolarizability and enable efficient two-photon absorption, we investigated their two-photon absorption behavior. Our findings indicated that all three luminogens exhibit two-photon activity in both molecular aggregates and crystalline forms (Fig. 4a–c and Fig. S23, ESI†). The two-photon excited emission spectra (excited at 845 nm) for these aggregates and crystals closely resemble the single-photon excited emission spectra (excited at 420 nm) (Fig. S21, ESI†). The emission spectra are also found to be anti-Stokes shifted, with excitation occurring in the 690 nm to 1100 nm range (Fig. S22 and S23, ESI†). Furthermore, a power-dependent two-photon emission intensity plotted in the log–log scale shows a slope of approximately 2 (Fig. S22 and S23, ESI†), suggesting a minimal contribution from the first-order emission. Additionally, two-photon cell imaging experiments demonstrated that our luminogens effectively illuminate cells, particularly the cytoplasmic region (Fig. 4d–l), verified against a control experiment (Fig. S24, ESI†). We also assessed
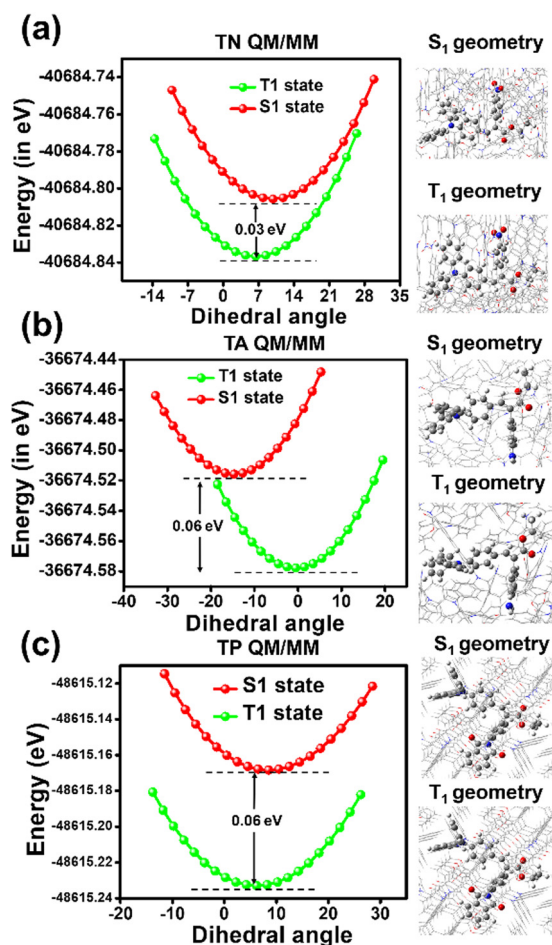

Fig. 2 Potential energy scanning along the dihedral angle (Fig. S13, ESI†) between donor and acceptor moieties in the crystal phase using the QM/MM model for (a) **TN**, (b) **TA**, and (c) **TP**. Here the QM layer has been treated at the B3LYP, 6-31G(d,p) level of theory, while the MM layer has been treated with a classical UFF level of theory.
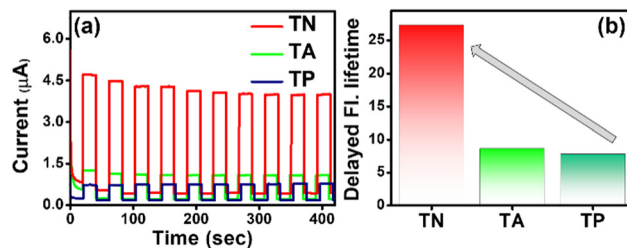

Fig. 3 (a) Photocurrent generation by the luminogens upon exciting with a 365–370 nm 60 W UV LED lamp having peak irradiance of 3.5 W cm^{-2}. (b) Neat film DF lifetime of the luminogens.
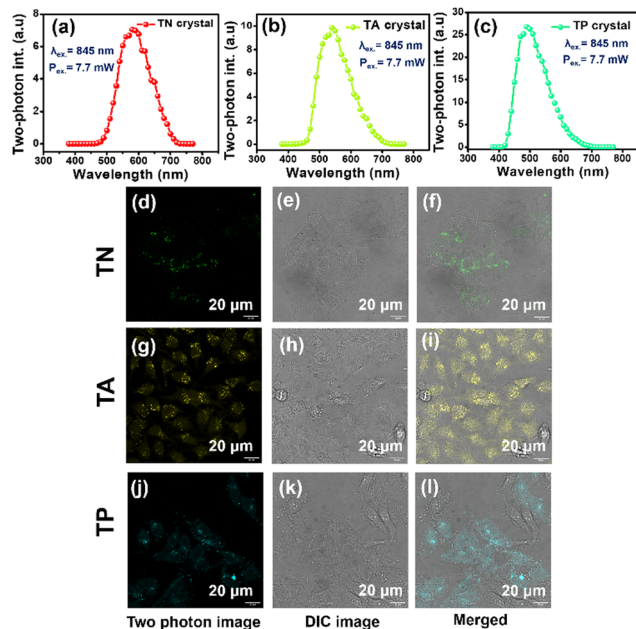
Fig. 4 Two-photon excited emission spectra (ex. 845 nm, power = 7.7 mW) of (a) **TN**, (b) **TA** and (c) **TP** crystals. Two-photon microscopy image (excitation wavelength = 820 nm, collection window is from 600 nm to 630 nm for **TN**, 505 nm to 535 nm for **TA**, and 540 to 580 for **TP**) of HeLa cells: (d), (g) and (j) dye treated two-photon imaging, (e), (h) and (k) differential interference contrast (DIC) images, and (f), (i) and (l) DIC image merged with dye-treated confocal images.

the cytotoxicity of our luminogens using the MTT cell viability assay on HeLa cells. The results, confirmed across three biological replicates, show no significant cell death (viability remains over 80%) with drug concentrations up to 15 μM (Fig. S25, ESI†), indicating that the luminogens are not toxic to cells at these levels.

In summary, we report three donor–acceptor-based luminogens **TN**, **TA**, and **TP** with aggregation-induced delayed fluorescence (AIDF) properties. The combined solvent phase and QM/MM-based calculation reveal a drastic lowering of the ΔE_{ST} values in the aggregated state, responsible for the observed behavior. Their strong charge-transfer nature and AIDF characteristics have been used to increase singlet exciton diffusion length for efficient photo-current generation. Additionally, their promising two-photon absorption capabilities demonstrate their potential for anti-Stokes shifted photoluminescence (ASPL) and two-photon cell imaging.

Data availability

The data supporting this article have been included as a part of the ESI.†

Conflicts of interest

There are no conflicts to declare.

Notes and references

1 (a) H. Uoyama, K. Goushi, K. Shizu, H. Nomura and C. Adachi, *Nature*, 2012, **492**, 234–238; (b) Y. Tao, K. Yuan, T. Chen, P. Xu, H. Li, R. Chen, C. Zheng, L. Zhang and W. Huang, *Adv. Mater.*, 2014, **26**, 7931–7958; (c) G. Hong, X. Gan, C. Leonhardt, Z. Zhang, J. Seibert, J. M. Busch and S. Bräse, *Adv. Mater.*, 2021, **33**, 2005630; (d) T.-L. Wu, M.-J. Huang, C.-C. Lin, P.-Y. Huang, T.-Y. Chou, R.-W. Chen-Cheng, H.-W. Lin, R.-S. Liu and C.-H. Cheng, *Nat. Photonics*, 2018, **12**, 235–240; (e) K. Bergmann, R. Hojo and Z. M. Hudson, *J. Phys. Chem. Lett.*, 2023, **14**, 310–317; (f) X.-K. Chen, D. Kim and J.-L. Brédas, *Acc. Chem. Res.*, 2018, **51**, 2215–2224; (g) P. Data, P. Pander, M. Okazaki, Y. Takeda, S. Minakata and A. P. Monkman, *Angew. Chem., Int. Ed.*, 2016, **55**, 5739–5744; (h) X.-K. Chen, Y. Tsuchiya, Y. Ishikawa, C. Zhong, C. Adachi and J.-L. Brédas, *Adv. Mater.*, 2017, **27**, 1702767.

2 (a) J. Xu, X. Zhu, J. Guo, J. Fan, J. Zeng, S. Chen, Z. Zhao and B. Z. Tang, *ACS Mater. Lett*, 2019, **1**, 613–619; (b) J. Liu, J. Fan, K. Zhang, Y. Zhang, C.-K. Wang and L. Lin, *Chin. Phys. B*, 2020, **29**, 088504; (c) D. Barman and P. K. Iyer, *J. Phys. Chem. C*, 2023, **127**, 2694–2704.

3 (a) J. Luo, Z. Xie, J. W. Y. Lam, L. Cheng, H. Chen, C. Qiu, H. S. Kwok, X. Zhan, Y. Liu, D. Zhuc and B. Z. Tang, *Chem. Commun.*, 2001, 1740–1741; (b) G. R. Suman, M. Pandey and A. S. J. Chakravarthy, *Mater. Chem. Front.*, 2021, **5**, 1541–1584; (c) J. Mei, Y. Hong, J. W. Y. Lam, A. Qin, Y. Tang and B. Z. Tang, *Adv. Mater.*, 2014, **26**, 5429–5479; (d) P.-A. Yin, Q. Wan, Y. Niu, Q. Peng, Z. Wang, Y. Li, A. Qin, Z. Shuai and B. Z. Tang, *Adv. Electron. Mater.*, 2020, **6**, 2000255; (e) H. Wang, Q. Gong, G. Wang, J. Dang and F. Liu, *J. Chem. Theory Comput.*, 2019, **15**, 5440–5447; (f) R. C.-Otero, Q. Li and L. Blancafort, *Chem. – Asian J.*, 2019, **14**, 700–714.

4 (a) Y. Matsui, Y. Yokoyama, T. Ogaki, K. Ishiharaguchi, A. Niwa, E. Ohta, M. Saigo, K. Miyata, K. Onda, H. Naito and H. Ikeda, *J. Mater. Chem. C*, 2022, **10**, 4607–4613; (b) J. Fan, L. Lin and C.-K. Wang, *J. Mater. Chem. C*, 2017, **5**, 8390–8399; (c) N. Aizawa, C.-J. Tsou, I. S. Park and T. Yasuda, *Polym. J.*, 2017, **49**, 197–202; (d) B. Zhang, Y. Kong, H. Liu, B. Chen, B. Zhao, Y. Luo, L. Chen, Y. Zhang, D. Han, B. Z. Tang and L. Niu, *Chem. Sci.*, 2021, **12**, 13283.

5 D. Liu, M. Zhang, W. Tian, Y. Sun, Z. Zhao and B. Z. Tang, *Aggregate*, 2022, **3**, e164.

6 G. Li, J. Pu, Z. Yang, H. Deng, Y. Liu, Z. Mao, J. Zhao, S.-J. Su and Z. Chi, *Aggregate*, 2023, **4**, e382.

7 R. Furue, T. Nishimoto, I. S. Park, J. Lee and T. Yasuda, *Angew. Chem., Int. Ed.*, 2016, **55**, 7171–7175.

8 S.-L. Lai, Q.-X. Tong, M.-Y. Chan, T.-W. Ng, M.-F. Lo, S.-T. Lee and C.-S. Lee, *J. Mater. Chem.*, 2011, **21**, 1206–1211.

9 T. J. Penfold, F. B. Dias and A. P. Monkman, *Chem. Commun.*, 2018, **54**, 3926–3935.

10 C. Deibel, Photocurrent Generation in Organic Solar Cells, *Semicond. Semimetals*, 2011, **85**, 297–330.

11 (a) Q. Lu, C.-J. Wu, Z. Liu, G. Niu and X. Yu, *Front. Chem.*, 2020, **8**, 617463; (b) Y. Wang, H. Wu, P. Li, S. Chen, L. O. Jones, M. A. Mosquera, L. Zhang, K. Cai, H. Chen, X.-Y. Chen, C. L. Stern, M. R. Wasielewski, M. A. Ratner, G. C. Schatz and J. F. Stoddart, *Nat. Commun.*, 2020, **11**, 4633; (c) L. Xu, J. Zhang, L. Yin, X. Long, W. Zhanga and Q. Zhang, *J. Mater. Chem. C*, 2020, **8**, 6342–6349; (d) T. Liu, L. Xu, H. Wang, B. Chen and S. Shi, *ACS Appl. Bio Mater.*, 2023, **6**, 2849–2859.

12 (a) A. Chatterjee, J. Chatterjee, S. Sappati, T. Sheikh, R. M. Umesh, M. D. Ambhore, M. Lahiri and P. Hazra, *J. Phys. Chem. B*, 2021, **125**, 12832–12846; (b) A. Chatterjee, J. Chatterjee, S. Sappati, R. Tanwar, M. D. Ambhore, H. Arfin, R. M. Umesh, M. Lahiri, P. Mandal and P. Hazra, *Chem. Sci.*, 2023, **14**, 13832–13841.